


Article

The Effect of Ultraviolet Treatment on TiO₂ Nanotubes: A Study of Surface Characteristics, Bacterial Adhesion, and Gingival Fibroblast Response

Masahiko Kobayashi^{1,2}, Aous A. Abdulmajeed³, Jongyun Moon², Khalil Shahramian^{2,4,*} , Risto Punkkinen⁵, Jun Shimada⁶, Pekka K. Vallittu^{7,8} and Lippo V. Lassila^{2,7}

- ¹ Division of Geriatric Dentistry, School of Dentistry, Meikai University, Keyakidai, Sakado 350-0283, Japan; kobayashimasahiko19830723@gmail.com
 - ² Turku Clinical Biomaterials Centre (TCBC), University of Turku, 20520 Turku, Finland; jongyun.moon@gmail.com (J.M.); liplas@utu.fi (L.V.L.)
 - ³ Department of General Practice, School of Dentistry, Virginia Commonwealth University, Richmond, VA 23298-0566, USA; aabdulmajeed@vcu.edu
 - ⁴ Department of Prosthetic Dentistry and Stomatognathic Physiology, Institute of Dentistry, University of Turku, 20520 Turku, Finland
 - ⁵ Department of Computing, University of Turku, 20014 Turku, Finland; rpunk@utu.fi
 - ⁶ Division of Oral and Maxillofacial Surgery, Meikai University, Keyakidai, Sakado 350-0283, Japan; shimadajun@mac.com
 - ⁷ Department of Biomaterials Science, Institute of Dentistry, University of Turku, 20520 Turku, Finland; pekval@utu.fi
 - ⁸ City of Turku Welfare Division, Oral Health Care, 20101 Turku, Finland
- * Correspondence: khalsha@utu.fi



Citation: Kobayashi, M.; Abdulmajeed, A.A.; Moon, J.; Shahramian, K.; Punkkinen, R.; Shimada, J.; Vallittu, P.K.; Lassila, L.V. The Effect of Ultraviolet Treatment on TiO₂ Nanotubes: A Study of Surface Characteristics, Bacterial Adhesion, and Gingival Fibroblast Response. *Metals* **2022**, *12*, 80. <https://doi.org/10.3390/met12010080>

Academic Editors: Sina Jamali and Mieczysław Jurczyk

Received: 24 November 2021

Accepted: 28 December 2021

Published: 4 January 2022

Publisher's Note: MDPI stays neutral with regard to jurisdictional claims in published maps and institutional affiliations.



Copyright: © 2022 by the authors. Licensee MDPI, Basel, Switzerland. This article is an open access article distributed under the terms and conditions of the Creative Commons Attribution (CC BY) license (<https://creativecommons.org/licenses/by/4.0/>).

Abstract: Titanium dioxide (TiO₂) nanotubes are emerging as a provocative target for oral implant research. The aim of this study was to evaluate the effect of UV on the wettability behavior, bacterial colonization, and fibroblast proliferation rate of TiO₂ nanotube surfaces prepared using different anodization voltages and aimed for use as implant abutment materials. Four different experimental materials were prepared: (1) TiO₂ nanotube 10 V; (2) TiO₂ nanotube 15 V; (3) TiO₂ nanotube 20 V; and (4) commercial pure titanium as a control group. TiO₂ nanotube arrays were prepared in an aqueous electrolyte solution of hydrofluoric acid (HF, 0.5 vol.%). Different anodization voltages were used to modify the morphology of the TiO₂ nanotubes. Equilibrium contact angles were measured using the sessile drop method with a contact angle meter. The investigated surfaces ($n = 3$) were incubated at 37 °C in a suspension of *Streptococcus mutans* (*S. mutans*) for 30 min for bacterial adhesion and 3 days for biofilm formation. Human gingival fibroblasts were plated and cultured on the experimental substrates for up to 7 days and the cell proliferation rate was assessed using the AlamarBlue assayTM (BioSource International, Camarillo, CA, USA). The data were analyzed using one-way ANOVA followed by Tukey's post-hoc test. Water contact angle measurements on the TiO₂ after UV treatment showed an overall hydrophilic behavior regardless of the anodization voltage. The ranking of the UV-treated surfaces of experimental groups from lowest to highest for bacterial adhesion was: TiO₂ nanotube 20 V < Ti and TiO₂ nanotube 15 V < TiO₂ nanotube 10 V ($p < 0.05$), and for bacterial biofilm formation was: TiO₂ nanotube 20 V-TiO₂ nanotube 10 V < Ti-TiO₂ nanotube 15 V ($p < 0.05$). Fibroblast cell proliferation was lower on TiO₂ nanotube surfaces throughout the incubation period and UV light treatment showed no enhancement in cellular response. UV treatment enhances the wettability behavior of TiO₂ nanotube surfaces and could result in lower bacterial adhesion and biofilm formation.

Keywords: metallic biomaterials; organic and inorganic coatings; UV treatment; TiO₂; nanotubes; bacterial colonization; fibroblast proliferation rate

1. Introduction

Titanium and its alloys are the biomaterials of choice in implant dentistry. The different components of a dental implant contact different environments. The implant fixture is in contact with bone, the implant neck and platform have a soft tissue transgingival interface, and the supragingival crown component makes contact with the salivary oral cavity environment. Therefore, the surfaces of different implant components need to be optimized to respond favorably to the corresponding interface. Over the last few decades, studies have been focused on researching the osseointegration of oral implants. While the osseointegration of current oral implants is certain, research interest has been directed towards the soft tissue cuff around abutments [1–4]. A true bond with the surrounding soft tissue is known to provide a seal that prevents bacteria in the oral cavity from infecting the peri-implant tissue, thereby playing a major role in preventing peri-implant infections [1–4].

The challenge faced in modifying dental implant surfaces is the race between bacterial colonization and tissue integration on the same surface after implantation. Cellular behaviors (i.e., adhesion, morphological change, functional alteration, and proliferation) are mainly influenced by surface characteristics of the implant surface such as roughness, hydrophilicity, charge, free energy, and morphology [3,5–12]. Studies have shown that surface free energy (SFE) is a more critical surface characteristic than surface roughness for cellular adhesion strength and proliferation, and that the SFE components of the various materials tested are related to cellular adhesion strength [13,14]. Nevertheless, it has been reported that roughness coupled with SFE affects the biological behavior of materials [14]. Therefore, surface modifications at the nano-level can be utilized to control such material properties [14].

Many surface modifications have been studied to modify and thus improve biological responses to implant surfaces [15–18]. Titanium dioxide (TiO₂) nanotubes are emerging as a provocative target for oral implant research [19,20]. TiO₂ nanotubes are synthesized electrochemically on the surface of titanium by anodization in a fluoride-containing electrolyte [21]. Previous research has shown that titanium nanotubes possess the ability to enhance the adhesion and differentiation of different eukaryotic cells, including osteoblasts [21]. However, it has been reported that the surfaces either suppress or promote the adhesion of bacteria [21]. Furthermore, research has shown that TiO₂ nanotubes may stimulate bone growth around oral implants [22,23]. However, to date, research on the effects of nanotubes on cells building oral connective tissue is scarce.

Another method for titanium surface optimization is ultraviolet (UV) irradiation, which has been proven to significantly enhance the osteoconductive capacity of titanium surfaces and to have antibacterial effects [24,25]. UV photofunctionalization of titanium surfaces has been found to increase hydrophilicity and protein adsorption [26]. In addition, UV irradiation substantially enhances the osteoconductive capacity of titanium [27]. Furthermore, research on the effects of UV on the nanostructural surfaces of titanium has shown it to increase the level of bone-like apatite formation in simulated body fluids [28]. Despite the extensive research on the effects of UV on integration with bone, the effects of UV on soft tissue attachment still remain uncertain.

Although existing research reports the osteoconductive potential of titanium nanotubes, it is important to study how implant neck and abutments can be optimized for better soft-tissue adherence while minimizing or avoiding bacterial colonization. Accordingly, the aim of this study was to evaluate the effects of UV on wettability behavior and biocompatibility, in terms of bacterial colonization and cell proliferation on TiO₂ nanotube surfaces prepared using different anodization voltages—aimed for use as an implant abutment material. Since the main component of the gingival connective tissue is gingival fibroblasts, this study focused on evaluating fibroblast cell proliferation on different surface modifications of titanium. Colonization of the surfaces by *Streptococcus mutans* was studied. *S. mutans* biofilm is considered to be an important prerequisite for the adhesion of other bacterial species involved in periodontal disease [29].

2. Materials and Methods

2.1. Specimen Preparation

Four different experimental groups were prepared based on their anodization voltage: (1) Grade I pure Ti (control), (2) TiO₂ nanotubes 10 V, (3) TiO₂ nanotubes 15 V, and (4) TiO₂ nanotubes 20 V. The size of the specimen was 10 mm × 10 mm × 0.3 mm. Anodization was performed as follows: Grade I Ti foil (20 mm × 20 mm × 0.1 mm, 99.5%) was used as an anode substrate to fabricate TiO₂ nanotube arrays, and a platinum foil (20 mm × 20 mm × 0.1 mm, 99.98%) was used as a cathode. The Ti foil was ultrasonicated in deionized (DI) water, acetone, and isopropanol, and dried in an air stream. All specimens were anodized in an electrolyte containing 0.5 vol. % hydrogen fluoride in DI at room temperature (22 °C) for 40 min. In order to modify the morphological structure of the nanotubes, different constant anodization voltages of 10, 15, and 20 V were applied [30]. After anodization, the specimens were immediately rinsed with DI water and dried in an air stream. Two different sets of specimens were then prepared, with and without UV treatment. Subsequently, the UV light treatment was performed using at a distance of 15 cm under a UV-A lamp (300–400 nm wavelength; Sylvania Blacklight-Blue, F 15 W/BLB-TB, Osram, Munich, Germany) for 24 h.

2.2. Field Emission Scanning Electron Microscopy (FESEM)

The surface morphology structure of the TiO₂ nanotube surfaces at different anodization voltages was observed using FESEM (S-4800, Hitachi, Tokyo, Japan). The cross-sectional images of the TiO₂ tubes were taken from lifted layers, which were obtained by mechanical bending of the specimens. The geometrical features (i.e., pore diameter and tube length) were measured by FESEM.

2.3. Surface Roughness Measurements

The surface roughness parameters of the specimens ($n = 3$) were determined by image analysis (Vision 5.41 software) of the micrographs obtained from a 3D optical profiler (ContourGT-K, Bruker, Billerica, MA, USA) with a vertical resolution of 0.1 nm. The analyzed images were taken using white light interferometry (WLI) technology with a minimum lateral resolution of 0.38 μm, sample slope of 40 degrees, at ×100 magnification, and with a measurement area of X: 63.3 μm × Y: 47.4 μm.

2.4. Contact Angle Measurements

Equilibrium contact angles (θ_C) were measured using the sessile drop method (described in detail elsewhere [31]) with a contact angle meter (KSV-CAM100, KSV Instruments LTD., Helsinki, Finland). A drop was deposited on the surface and imaged for 20 s by collecting one image per 2 s. Determination of contact angles was based on the Young–Laplace equation, yielding the contact angles on both sides of the droplet and their mean values. Three liquids were used as a probe for SFE calculations (Table 1). The result was the mean of at least 6 drops on each specimen.

Table 1. Test liquids and their surface tension components adapted from [32].

Liquid	Source	Surface Tension (mN/m)			
		γ^{TOT}	γ^{D}	γ^+	γ^-
Distilled water, ultrapure water Milli-Q	Produced in-house	72.8	21.8	25.5	25.5
Diiodomethane > 99% purity	Sigma-Aldrich, St. Louis, CA, USA	50.8	50.8	0	0
Formamide, pro analysis	Merck, Darmstadt, Germany	58	39	2.28	39.6

2.5. Surface Free Energy Calculations

The SFE was calculated using the Owens–Wendt (OW) approach. The OW model approach gives the long-range dispersion (Lifshitz–van der Waals; γ^{D}) and the short-range polar (hydrogen bonding; γ^{P}) components of the SFE [31]. The spreading pressure was not

taken into account as it contributes to SFE and has to be considered if the SFE is higher than 60 mJ/m^2 [33]. In the present work, SFE values were lower than this limit and thus, the spreading pressure could be disregarded.

2.6. Bacterial Response

2.6.1. Cultivation of *Streptococcus mutans* and Preparation of Cell Suspensions

For the adhesion experiments, *Streptococcus mutans* (*S. mutans*) Ingbritt was cultured on blood plates (Orion Diagnostica, Espoo, Finland) for 16 h at 37°C in an anaerobic atmosphere. In these conditions, the cells occur in suspension as singles, pairs, or triplets, which makes further homogenization unnecessary [34]. The cells were harvested from the plates with plastic loops, washed twice ($10,000\times g$, 10 min) with phosphate-buffered saline (PBS; 137 mM NaCl, 10 mM phosphate, 2.7 mM KCl, pH 7.4), and suspended in the adsorption buffer to an optical density of 0.35 (A_{550}), corresponding to 5×10^8 colony-forming units (CFU) per mL [34].

2.6.2. Adhesion Tests

The adhesion experiments were essentially performed as described earlier [34]. The discs ($n = 3$) were first preincubated in 2 mL adsorption buffer/diluted saliva at room temperature for 30 min using gentle rolling (The Coulter Mixer, Luton, UK) in 14 mL capped plastic test tubes with an inner diameter of 16 mm (Falcon, BD Biosciences, Bedford, MA, USA). The mixer was tilted at a 15-degree angle to ensure that the discs were covered by liquid at all times. After the preincubation, the discs were rinsed once in 50 mL saline (0.9% NaCl, Orion Diagnostica, Espoo, Finland) and then transferred to test tubes with 2 mL of the cell suspension, prepared as described above. The discs were rolled in the cell suspensions for 30 min and then rinsed gently 3 times in 50 mL saline. Thereafter, the attached cells from one side of the disc were scraped into 0.5 mL of transport medium (Tryptic Soy Broth, Difco Laboratories, MI, USA). Three applicators that were dipped into fresh transport medium before the procedure (Quick-Stick, Dentsolv AB, Saltsjö-boo, Sweden) were used to scrape the cells from the disc. The brush ends of the applicators were cut into the transport media. In preliminary experiments, one Vortex-treatment of the vials efficiently removed the bacteria from brushes 1 and 2; increasing the number of scrapings from 3 to 4 did not increase the cell yield. The same method has been used to collect early plaque formed on different materials [35].

For the enumeration of cells on the disc surfaces as colony-forming units, the vials with the microbe samples collected from the surfaces were thoroughly Vortex-treated and, after serial dilutions of the samples, grown anaerobically for 3 days at 37°C on Mitis salivarius agars (Difco™, Becton, Dickinson and Company, Franklin Lakes, NJ, USA).

2.6.3. Biofilm Formation Test

S. mutans biofilm formation was tested by a modification of the method originally presented by Ebi et al. [36]. The microorganism we used was the reference strain *Streptococcus mutans* Ingbritt. It was first grown overnight in Brain Heart Infusion medium (BHI; Becton Dickinson and Company, Sparks, MD, USA). After 24 h, the cells were washed with phosphate-buffered saline ($5000\times g$, 10 min) and then they were suspended in BHI containing 1% sucrose ($A_{550} = 0.05$). This suspension (500 μL) was pipetted onto the experimental discs placed in the wells of cell culture plates. The plates were incubated anaerobically (90% N_2 , 5% CO_2 , 5% H_2) at 37°C for 24 h. The biofilms were collected with microbrushes (Quick-Stick®, Dentsolv AB, Saltsjö-Boo, Sweden) from the disc surface exposed to the medium. The microbrushes were then placed into test tubes containing Tryptic Soy Broth (Becton Dickinson and Company, Franklin Lakes, NJ, USA). The tubes were vortexed and mildly sonicated and then serially diluted for plate culturing of *S. mutans*. The plates were grown for 3 days anaerobically (80% N_2 , 10% CO_2 , 10% H_2) at 37°C on Mitis salivarius agar (Becton Dickinson and Company, Franklin Lakes, NJ, USA), the colonies were counted under a stereomicroscope, and the results were expressed as CFU/disc surface. The biofilm

collection method has been tested in our earlier studies and it is highly reproducible [35,37]. In some experiments, the materials were subjected to fixation followed by SEM, as described in the following.

2.7. Cell Proliferation

Fibroblasts initiated from healthy human gingival biopsy samples were maintained in Dulbecco's Modified Eagle Medium (DMEM) supplemented with 10% fetal bovine serum and 100 U/ μ g penicillin–streptomycin (Gibco BRL, Life Technologies, Paisley, UK), and incubated at 37 °C in a 5% CO₂ environment. Semi-confluent cultures were trypsinized, and the cells were counted and resuspended in complete culture medium. The culture medium was changed three times a week.

The proliferation of cultured cells was determined using the AlamarBlue™ assay (BioSource International, Camarillo, CA, USA) in colorimetric format. Fibroblasts were plated at a density of 10,000 cells/cm² on the substrates investigated and cultured for up to 7 days. The substrates ($n = 6$) were withdrawn from the culture, at predetermined times (i.e., 1, 4, and 7 days), and placed into sterile culture plates containing fresh culture medium with 10% assay reagent. After 3 h of incubation, the absorbance values were read at 570 nm and 595 nm using an ELISA plate reader (Multiskan MS, Labsystems, Helsinki, Finland). Measured absorbances were used to calculate the reduction of the assay reagent, and the cell proliferation rate was normalized in respect to the proliferation rate of the pure titanium control (before UV-treatment) at the first time-point, which was arbitrarily set to 100%. A linear relationship between the cell number and absorbance readings was established using tissue culture polystyrene substrates.

2.8. Statistical Analysis

Statistical analysis was performed using GraphPad® Instat 3.05 software (GraphPad Software Inc., San Diego, CA, USA). The data were analyzed using one-way analysis of variance (ANOVA) followed by Tukey's post-hoc test. Differences were considered significant at a 95% confidence level.

3. Results

3.1. Scanning Electron Microscopy

Figure 1 shows the surface and cross-sectional FESEM images of the morphology of TiO₂ nanotubes prepared using different anodization voltages. The geometrical features (i.e., pore diameter and tube length) are summarized in Table 2. The pore diameter and tube length increased significantly ($p < 0.001$) with increasing anodization voltage.

Table 2. The morphology parameters (pore diameter and tube length) of TiO₂ nanotube arrays at different voltages ($n = 3$). Different superscript letters within the value indicate statistically different subsets.

Voltage (V)	Pore Diameter (nm) Mean (SD)	Tube Length (nm) Mean (SD)
TiO ₂ nanotube 10 V	42.2 (0.6) ^a	225 (21.2) ^a
TiO ₂ nanotube 15 V	67.6 (4.0) ^b	260.3 (4.5) ^b
TiO ₂ nanotube 20 V	117 (2.6) ^c	360 (4.3) ^c

3.2. Surface Roughness Parameters

The surface roughness parameters of the investigated specimens are shown in Table 3.

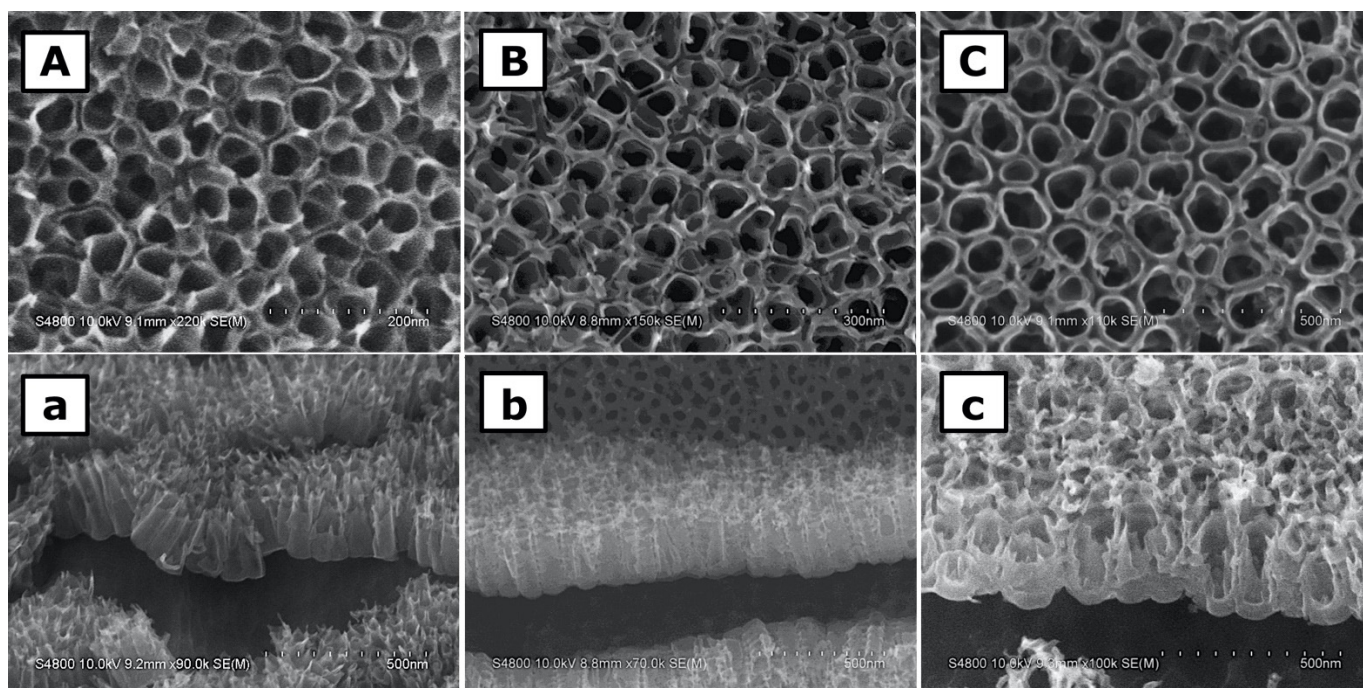


Figure 1. FE-SEM images showing top view and cross-section of TiO₂ nanotube arrays anodized at (A,a) 10 V, (B,b) 15 V, and (C,c) 20 V.

Table 3. Mean values and standard deviations (SD) of the specimens' surface roughness parameters recorded with a 3D optical profiler in micrometers. Roughness average Ra is the arithmetic mean of the absolute values of the roughness profile ordinates. Rp is the maximum peak height of the roughness profile within one sampling length. Root mean square deviation Rq indicates the root mean square along the sampling length. Rt is the vertical distance between the maximum profile peak height and the maximum profile valley depth along the evaluation length. Rv is the maximum valley depth of the roughness profile within one sampling length (previously, the parameter symbol Rm was used in place of Rv).

	Ra (μm)	Rp (μm)	Rq (μm)	Rt (μm)	Rv (μm)
Ti	0.45 (0.01)	1.92 (0.18)	0.54 (0.01)	3.72 (0.16)	−1.80 (0.19)
TiO ₂ nanotube 10 V	0.63 (0.04)	2.19 (0.11)	0.74 (0.03)	4.82 (0.40)	−2.63 (0.50)
TiO ₂ nanotube 15 V	0.27 (0.03)	1.65 (0.13)	0.34 (0.03)	2.72 (0.25)	−1.07 (0.20)
TiO ₂ nanotube 20 V	0.37 (0.03)	1.91 (0.33)	0.46 (0.04)	3.58 (0.36)	−1.67 (0.22)

3.3. Contact Angle Measurements

Table 4 gives the equilibrium contact angles of the surfaces investigated. Regardless of the anodization voltage or UV treatment, TiO₂ nanotubes statistically enhanced the hydrophilicity of the titanium surfaces ($p < 0.001$). After UV treatment, all TiO₂ nanotube surfaces showed a total hydrophilic behavior corresponding to a contact angle of $<0.1^\circ$.

Table 4. Mean values and standard deviations (SD) of contact angle measurements. Values reported are degrees (θC).

Groups	Before UV Treatment (θC)			After UV Treatment (θC)		
	Water	Diiodomethane	Formamide	Water	Diiodomethane	Formamide
Ti	89.2 (2.1)	52.1 (3.4)	57.9 (8.0)	83.0 (1.7)	48.1 (1.6)	59.2 (4.5)
TiO ₂ nanotube 10 V	16.2 (2.1)	9.4 (1.4)	11.3 (0.6)	<0.1	<0.1	<0.1
TiO ₂ nanotube 15 V	22.4 (2.6)	12.7 (1.2)	17.5 (1.7)	<0.1	<0.1	<0.1
TiO ₂ nanotube 20 V	16.0 (2.0)	8.9 (1.9)	12.8 (3.1)	<0.1	<0.1	<0.1

3.4. Surface Free Energy Calculations

Table 5 gives the SFE components of the investigated surfaces. Regardless of the anodization voltage, TiO₂ nanotubes on titanium surfaces exhibited higher SFE than titanium controls.

Table 5. Mean values (mJ/m²) of surface free energy (SFE) components calculated using the Owens–Wendt approach.

Groups	Before UV Treatment			After UV Treatment		
	Dispersive SFE (γ ^D mJ/m ²)	Polar SFE (γ ^P mJ/m ²)	Total SFE (γ ^{TOT} mJ/m ²)	Dispersive SFE (γ ^D mJ/m ²)	Polar SFE (γ ^P mJ/m ²)	Total SFE (γ ^{TOT} mJ/m ²)
Ti	34.68	1.94	36.62	34.47	3.39	37.85
TiO ₂ nanotube 10 V	42.14	29.43	71.57	N/A	N/A	N/A
TiO ₂ nanotube 15 V	41.75	27.75	69.49	N/A	N/A	N/A
TiO ₂ nanotube 20 V	42.06	29.46	71.52	N/A	N/A	N/A

3.5. Bacterial Adhesion and Biofilm Formation

The amount of adhered *S. mutans* on the specimens investigated before and after UV treatment is shown in Figure 2. UV treatment showed significant decreases in bacterial adhesion only on TiO₂ nanotube 15 V and 20 V. Ranking of the UV-treated experimental groups from lowest to highest bacterial adhesion was as follows: TiO₂ nanotube 20 V < Ti and TiO₂ nanotube 15 V < TiO₂ nanotube 10 V ($p < 0.05$). No relation was found between surface roughness and the colonization of *S. mutans*.

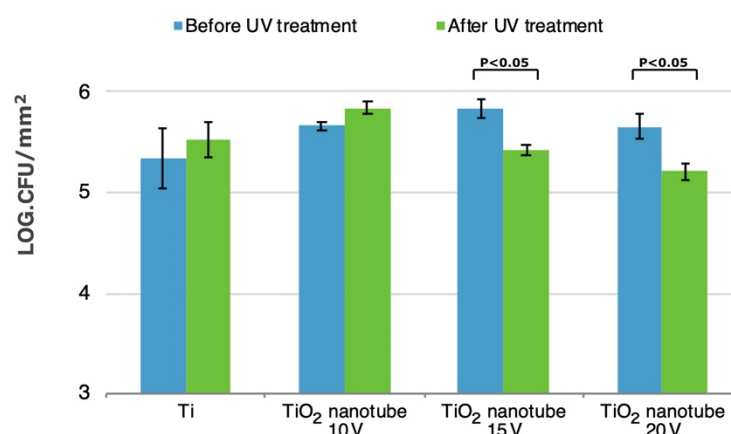


Figure 2. The amount of adhered *S. mutans* on the experimental specimens before and after UV treatment. Data are presented as mean \pm standard deviation ($n = 3$). UV treatment caused statistically significant decreases in bacterial adhesion only for 15 V and 20 V TiO₂ nanotubes.

The amount of *S. mutans* biofilm formation on the specimens investigated before and after UV treatment is shown in Figure 3. Before UV treatment, all TiO₂ nanotubes surfaces showed no statistical significance in comparison to Ti controls. Among the UV-treated specimens were used, decreased biofilm formation was found only on TiO₂ nanotube 20 V surfaces ($p < 0.01$). Comparing biofilm formation before and after UV treatment, there was a decrease on TiO₂ nanotube 10 V ($p < 0.01$) and on TiO₂ nanotube 20 V ($p < 0.05$).

3.6. Cell Proliferation

The fibroblast proliferation rates on the specimens investigated before and after UV treatment are shown in Figure 4. Throughout the culture period, all specimens showed a significant increase ($p < 0.001$) in cell proliferation rate before and after UV treatment.

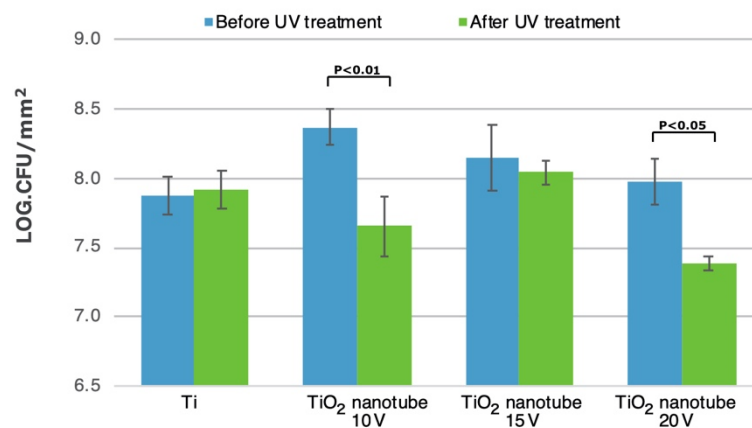


Figure 3. The amount of *S. mutans* biofilm formation on the experimental specimens before and after UV treatment. Data are presented as mean \pm standard deviation ($n = 4$). UV treatment caused statistically significant decreases in biofilm formation only for 10 V and 20 V TiO₂ nanotubes.

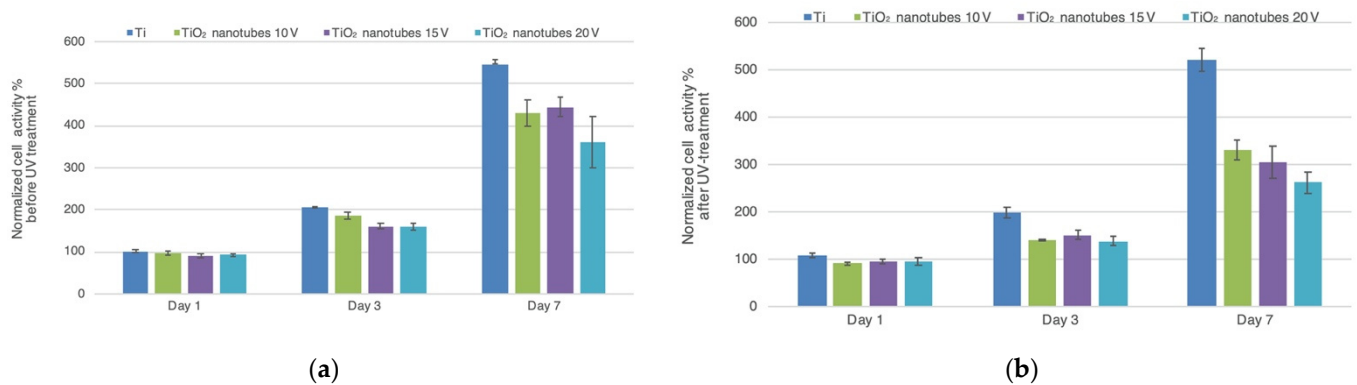


Figure 4. Proliferation of human gingival fibroblasts on the investigated specimens (a) before and (b) after UV-treatment. The reduction of AlamarBlue™ reagent with commercial pure titanium before UV-treatment substrate at the 1 d time-point was set to 100%. Data are presented as mean \pm standard deviation ($n = 6$).

Before UV treatment: By day 1, TiO₂ nanotube 15 V and 20 V showed lower cell proliferation rates than Ti controls ($p < 0.05$). By day 3, TiO₂ nanotube 10 V, 15 V, and 20 V showed lower cell proliferation rates than Ti controls ($p < 0.01$, $p < 0.001$, and $p < 0.001$, respectively). By day 7, TiO₂ nanotube 10 V, 15 V, and 20 V showed lower cell proliferation rates than Ti controls ($p < 0.001$).

After UV treatment: By day 1, TiO₂ nanotube 10 V, 15 V, and 20 V showed lower cell proliferation rates than Ti controls ($p < 0.001$, $p < 0.01$, and $p < 0.01$, respectively). By day 3 and 7, TiO₂ nanotube 10 V, 15 V, and 20 V showed lower cell proliferation rates than Ti controls ($p < 0.001$).

Comparing fibroblast proliferation rates before and after UV treatment, UV light caused a decrease in proliferation on TiO₂ nanotube 10 V and 20 V ($p < 0.01$) on day 3, and 10 V, 15 V, and 20 V ($p < 0.001$) on day 7.

4. Discussion

Osteoblasts play a crucial role in the osseointegration of oral implants; likewise, human gingival fibroblasts (HGFs) preserve the soft tissue integrity around the oral implant neck. Fibroblasts are the most common cells in the connective tissue that are responsible for the synthesis of fibers and other components of the ground substance, and therefore, HGFs are mainly used for in vitro studies evaluating peri-implant soft tissue reactions to different implant abutment materials [37]. Previous studies have focused on studying the reactions of bone cells and a few bacterial species to titanium nanotubes [37–41]. To the best of the

authors' knowledge, this study is among the first to examine the effect of UV treatment on fibroblast and *S. mutans* behavior on TiO₂ nanotube surfaces prepared using different anodization voltages aimed for use as implant abutment materials.

Anodic oxidation is a method for tailoring nanoscale-patterned surfaces for metals and alloys [42]. The diameter and distance between nanofeatures in addition to the shape or organization of these nanofeatures influence the cell response of implant surfaces [43,44]. Based on the literature, the optimum pore diameter of TiO₂ nanotubes should be less than 100 nm; however, the best diameter is still controversial [45]. Some studies report that pore diameters in the range 15–30 nm favor adhesion of different mammalian cells [41], while others report that 105 nm pores are favorable [38]. Similar differing results also are reported with bacterial colonization [21]. For instance, Narendrakumar et al. demonstrated that oral streptococci had the lowest adhesion with small-size TiO₂ nanotube diameters, while on the other hand, in a study by Peng et al., bacterial adhesion was reduced on larger 80 nm pores compared to smaller 30 nm ones [21,39]. This highlights the fact that the exact favorable parameters are still unknown in the literature. Nevertheless, the search for finding optimal parameters of different biomaterials for different clinical application continues. In our study, regardless of the pore diameter, TiO₂ nanotubes reduced fibroblast cell proliferation. Bacterial colonization results were in line with the results of Peng et al. [39], where the 20 V group with the largest pore diameter exhibited the lowest bacterial colonization after UV treatment. In the present study, the applied voltage seemed to play an important role in determining the morphology of the TiO₂ nanotube arrays and, subsequently, influenced cell responses. It may be inferred that the used methodology and voltages for constructing the reported nanotube diameters may not be optimal for enhancing the reaction of titanium to gingival fibroblasts. However, synergic with UV, TiO₂ nanotubes had lower bacterial adhesion.

UV photofunctionalization of titanium substantially improves the quality and strength of osseointegration by stimulating osteogenic cellular attachment and proliferation [27,28]. Furthermore, it also increases the hydrophilicity and protein adsorption of surfaces [26]. This improvement in osseointegration is accredited to the generation of superhydrophilic surfaces, a phenomenon that was first introduced in 1997 [46]. However, the mechanism of this superhydrophilic behavior is still unknown. Presently, two hypotheses have been proposed [27,47]: one is the generation of surface vacancies at bridging sites, resulting in the conversion of Ti⁴⁺ to Ti³⁺, which is favorable for dissociative water adsorption to form basic Ti–OH groups; the other is the elimination of hydrocarbons on the TiO₂ coating. The hydrophilic nature of any surface is an indicator of its surface energy and can determine to a great extent the biocompatibility level of materials via its effect on protein–material–cell interactions [48–50]. In accordance, our findings showed the UV light treatment resulted in an overall hydrophilic behavior for TiO₂ surfaces. It has been demonstrated, at both cellular and tissue levels [27,51–53], that UV-photofunctionalization promotes the osseointegration process on titanium surfaces to a greater extent than any other surface modifications, such as nanotopographical or chemical modification. However, the topographic and physicochemical properties of implant surfaces also play a fundamental role in the process of osseointegration [16].

It has been acknowledged that a certain threshold roughness (Ra around 0.2 μm) is essential for accomplishing a stable soft tissue seal around titanium implants. An increase in surface roughness of the transmucosal area above 0.2 μm will facilitate early plaque formation [54]. Therefore, an ideal transmucosal implant surface should allow epithelial and connective tissue attachment while simultaneously minimizing bacterial adhesion. However, in the present study, all the substrates showed rather rough surface characteristics (Ra more than 0.2 μm), because of the porous nature at the TiO₂ nanotube surface structure. Furthermore, it may be expected that the entrapment of air on rougher surfaces might result in higher water contact angles and lower wettability [21,55]. However, this effect was not observed in our study, as the rougher 10 V group had wettability values recorded in the same range as the 15 V and 20 V groups. With regards to the relation of roughness

on cell proliferation, Rosqvist et al. reported a direct correlation between roughness and fibroblast cell adhesion [56]. Fibroblasts reportedly proliferated more on rougher surfaces compared to smoother surfaces [56]. This phenomenon is also observed in our study, where relatively smoother experimental groups with TiO₂ nanotubes had lower gingival fibroblast proliferation when compared to Ti controls. Nevertheless, the results of in vitro tests are inconclusive, since cell interactions with biomaterials are influenced by several other factors coupled with surface roughness. The measurement of the sub-micron roughness of the specimens may be regarded as one limitation of this study. Measurements in the nanoscale may help infer more relatable conclusions, considering the nanostructure of the surfaces. Nevertheless, both the micro-roughness and the nano-roughness of dental implant materials is far from being standardized in the literature, and the power of predicting biological performances with these data is limited [14]. In order to address this issue, all the recorded roughness parameters were reported in the results of this study for better future reference. Our results indicated that UV light decreased *S. mutans* adhesion and biofilm formation despite the different surface roughnesses. However, TiO₂ nanotube surfaces that have higher surface energies compared to the titanium controls seemed to have similar or rather lower *S. mutans* colonization only after UV light treatment, thereby showing no influence of surface roughness on *S. mutans* adhesion. This is in accordance with Lippo et al., who found no correlation between surface roughness and the adhesion of *S. mutans* [57]. Although *S. mutans* is considered to be a pioneer species in oral biofilm formation [29], further studies are needed to focus on other bacteria—including *P. gingivalis* or *S. sanguis*—to overcome the limitations of this in vitro study, in which only one type of oral bacteria was used, and thus better simulate the oral environment.

The proliferation of fibroblasts was evaluated as an increase in metabolic activity and no absolute cell counts were determined. Although surfaces after UV treatment showed lower cellular activity, it might remain favorable to treat implant surfaces with UV light, as it is reported that UV treatment overcomes the time-related degrading bioactivity of titanium [58] that, in fact, could positively influence the prognosis of oral implant treatment. Proliferation data were also confirmed in the SEM analysis, which showed matching results for all substrate types (data not shown). Further research is required to address the exact mechanism by which UV affects gingival fibroblast cells.

In the current study, bacterial and cellular responses to TiO₂ nanotube surfaces were investigated under in vitro conditions, although soft tissue attachment in vivo occurs following complicated biological processes. Human gingival fibroblasts are commonly used in implant materials research. However, in real life, fibroblasts attach on surfaces via proteoglycan layers—a situation that cannot be mimicked in laboratory conditions. Thus, studies in real tissue environments are necessary for examining the in vivo behavior of TiO₂ nanotube surfaces before any conclusions can be made regarding their use as implant abutment materials.

5. Conclusions

Based on the findings of this study, it can be concluded that UV treatment enhances the wettability behavior of TiO₂ nanotube surfaces and could result in lower bacterial adhesion and biofilm formation. The proliferation of gingival fibroblasts was lower on the fabricated TiO₂ nanotubes when compared to controls. It may be inferred that the parameters (10 V, 20 V, 30 V) used to fabricate nanotubes with pore diameters in the range of 40 nm–120 nm may not enhance gingival cell proliferation.

Author Contributions: All authors, M.K., A.A.A., J.M., K.S., R.P., J.S., P.K.V. and L.V.L., contributed equally to conceptualization, methodology, software, validation, formal analysis, investigation, resources, data curation, writing—original draft preparation—review and editing, and visualization. Supervision, P.K.V., L.V.L. All authors have read and agreed to the published version of the manuscript.

Funding: This research received no external funding.

Conflicts of Interest: The authors declare no conflict of interest.

References

1. Abrahamsson, I.; Berglundh, T.; Glantz, P.-O.; Lindhe, J. The mucosal attachment at different abutments. *J. Clin. Periodontol.* **1998**, *25*, 721–727. [[CrossRef](#)]
2. Zitzmann, N.U.; Abrahamsson, I.; Berglundh, T.; Lindhe, J. Soft tissue reactions to plaque formation at implant abutments with different surface topography. *J. Clin. Periodontol.* **2002**, *29*, 456–461. [[CrossRef](#)] [[PubMed](#)]
3. Van Brakel, R.; Cune, M.S.; Van Winkelhoff, A.J.; De Putter, C.; Verhoeven, J.W.; Van Der Reijden, W. Early bacterial colonization and soft tissue health around zirconia and titanium abutments: An in vivo study in man. *Clin. Oral Implants Res.* **2010**, *22*, 571–577. [[CrossRef](#)]
4. Shahramian, K.; Gasik, M.; Kangasniemi, I.; Walboomers, X.F.; Willberg, J.; Abdulmajeed, A.; Närhi, T. Zirconia implants with improved attachment to the gingival tissue. *J. Periodontol.* **2019**, *91*, 1213–1224. [[CrossRef](#)] [[PubMed](#)]
5. Linkevicius, T.; Apse, P. Influence of abutment material on stability of peri-implant tissues: A systematic review. *Int. J. Oral Maxillofac. Implants* **2008**, *23*, 449–456. [[PubMed](#)]
6. Teughels, W.; Van Assche, N.; Sliepen, I.; Quirynen, M. Effect of material characteristics and/or surface topography on biofilm development. *Clin. Oral Implants Res.* **2006**, *17*, 68–81. [[CrossRef](#)]
7. Bürgers, R.; Gerlach, T.; Hahnel, S.; Schwarz, F.; Handel, G.; Gosau, M. In vivo and in vitro biofilm formation on two different titanium implant surfaces. *Clin. Oral Implants Res.* **2010**, *21*, 156–164. [[CrossRef](#)]
8. Al-Ahmad, A.; Wiedmann-Al-Ahmad, M.; Faust, J.; Bächle, M.; Follo, M.; Wolkewitz, M.; Hannig, C.; Hellwig, E.; Carvalho, C.; Kohal, R. Biofilm formation and composition on different implant materials in vivo. *J. Biomed. Mater. Res. Part B Appl. Biomater.* **2010**, *95B*, 101–109. [[CrossRef](#)]
9. Größner-Schreiber, B.; Griepentrog, M.; Haustein, I.; Müller, W.-D.; Briedigkeit, H.; Göbel, U.B.; Lange, K.-P. Plaque formation on surface modified dental implants. An in vitro study. *Clin. Oral Implants Res.* **2001**, *12*, 543–551. [[CrossRef](#)]
10. Quirynen, M.; Van Der Mei, H.C.; Bollen, C.M.L.; Bossche, L.H.V.D.; Doornbusch, G.I.; van Steenberghe, D.; Busscher, H.J. The Influence of Surface-Free Energy on Supra- and Subgingival Plaque Microbiology. An In Vivo Study on Implants. *J. Periodontol.* **1994**, *65*, 162–167. [[CrossRef](#)]
11. Hamdan, M.; Blanco, L.; Khraisat, A.; Tresguerres, I.F. Influence of Titanium Surface Charge on Fibroblast Adhesion. *Clin. Implants Dent. Relat. Res.* **2006**, *8*, 32–38. [[CrossRef](#)] [[PubMed](#)]
12. Hallab, N.J.; Bundy, K.J.; O'Connor, K.; Moses, R.L.; Jacobs, J.J. Evaluation of Metallic and Polymeric Biomaterial Surface Energy and Surface Roughness Characteristics for Directed Cell Adhesion. *Tissue Eng.* **2001**, *7*, 55–71. [[CrossRef](#)]
13. Schakenraad, J.M.; Busscher, H.J.; Wildevuur, C.R.H.; Arends, J. Thermodynamic aspects of cell spreading on solid substrata. *Cell Biophys.* **1988**, *13*, 75–91. [[CrossRef](#)]
14. Rupp, F.; Liang, L.; Geis-Gerstorf, J.; Scheideler, L.; Hüttig, F. Surface characteristics of dental implants: A review. *Dent. Mater.* **2018**, *34*, 40–57. [[CrossRef](#)] [[PubMed](#)]
15. Ogawa, T.; Ozawa, S.; Shih, J.-H.; Ryu, K.; Sukotjo, C.; Yang, J.-M.; Nishimura, I. Biomechanical Evaluation of Osseous Implants Having Different Surface Topographies in Rats. *J. Dent. Res.* **2000**, *79*, 1857–1863. [[CrossRef](#)]
16. Shalabi, M.; Gortemaker, A.; Hof, M.V.; Jansen, J.; Creugers, N. Implant Surface Roughness and Bone Healing: A Systematic Review. *J. Dent. Res.* **2006**, *85*, 496–500. [[CrossRef](#)]
17. Nguyen, T.T.; Moon, S.; Oh, T.; Park, I.; Lee, M.; Bae, T. The effect of APH treatment on surface bonding and osseointegration of Ti-6Al-7Nb implants: An in vitro and in vivo study. *J. Biomed. Mater. Res. Part B Appl. Biomater.* **2015**, *103*, 641–648. [[CrossRef](#)] [[PubMed](#)]
18. Nevins, M.; Camelo, M.; Nevins, M.L.; Schupbach, P.; Kim, D.M. Connective tissue attachment to laser-microgrooved abutments: A human histologic case report. *Int. J. Periodontics Restor. Dent.* **2012**, *32*, 385–392.
19. Mei, S.; Wang, H.; Wang, W.; Tong, L.; Pan, H.; Ruan, C.; Ma, Q.; Liu, M.; Yang, H.; Zhang, L.; et al. Antibacterial effects and biocompatibility of titanium surfaces with graded silver incorporation in titania nanotubes. *Biomaterials* **2014**, *35*, 4255–4265. [[CrossRef](#)]
20. Butt, A.; Hamlekhan, A.; Patel, S.; Royhman, D.; Sukotjo, C.; Mathew, M.; Shokuhfar, T.; Takoudis, C. A Novel Investigation of the Formation of Titanium Oxide Nanotubes on Thermally Formed Oxide of Ti-6Al-4V. *J. Oral Implants* **2015**, *41*, 523–531. [[CrossRef](#)]
21. Narendrakumar, K.; Kulkarni, M.; Addison, O.; Mazare, A.; Junkar, I.; Schmuki, P.; Sammons, R.; Igljč, A. Adherence of oral streptococci to nanostructured titanium surfaces. *Dent. Mater.* **2015**, *31*, 1460–1468. [[CrossRef](#)] [[PubMed](#)]
22. Wang, N.; Li, H.; Lü, W.; Li, J.; Wang, J.; Zhang, Z.; Liu, Y. Effects of TiO₂ nanotubes with different diameters on gene expression and osseointegration of implants in minipigs. *Biomaterials* **2011**, *32*, 6900–6911. [[CrossRef](#)] [[PubMed](#)]
23. Von Wilmsky, C.; Bauer, S.; Lutz, R.; Meisel, M.; Neukam, F.W.; Toyoshima, T.; Schmuki, P.; Nkenke, E.; Schlegel, K.A. In vivo evaluation of anodic TiO₂ nanotubes: An experimental study in the pig. *J. Biomed. Mater. Res. Part B Appl. Biomater.* **2009**, *89*, 165–171. [[CrossRef](#)]
24. Funato, A.; Yamada, M.; Ogawa, T. Success Rate, Healing Time, and Implant Stability of Photofunctionalized Dental Implants. *Int. J. Oral Maxillofac. Implants* **2013**, *28*, 1261–1271. [[CrossRef](#)]
25. Att, W.; Ogawa, T. Biological aging of implant surfaces and their restoration with ultraviolet light treatment: A novel understanding of osseointegration. *Int. J. Oral Maxillofac. Implants* **2012**, *27*, 753–761.

26. Hori, N.; Ueno, T.; Minamikawa, H.; Iwasa, F.; Yoshino, F.; Kimoto, K.; Lee, M.C.-I.; Ogawa, T. Electrostatic control of protein adsorption on UV-photofunctionalized titanium. *Acta Biomater.* **2010**, *6*, 4175–4180. [[CrossRef](#)] [[PubMed](#)]
27. Aita, H.; Hori, N.; Takeuchi, M.; Suzuki, T.; Yamada, M.; Anpo, M.; Ogawa, T. The effect of ultraviolet functionalization of titanium on integration with bone. *Biomaterials* **2009**, *30*, 1015–1025. [[CrossRef](#)] [[PubMed](#)]
28. Liu, X.; Zhao, X.; Li, B.; Cao, C.; Dong, Y.; Ding, C.; Chu, P.K. UV-irradiation-induced bioactivity on TiO₂ coatings with nanostructural surface. *Acta Biomater.* **2008**, *4*, 544–552. [[CrossRef](#)]
29. Viitaniemi, L.; Abdulmajeed, A.; Sulaiman, T.; Söderling, E.; Närhi, T. Adhesion and Early Colonization of *S. Mutans* on Lithium Disilicate Reinforced Glass-Ceramics, Monolithic Zirconia and Dual Cure Resin. *Eur. J. Prosthodont. Restor. Dent.* **2017**, *25*, 228–234. [[CrossRef](#)]
30. Macak, J.; Tsuchiya, H.; Ghicov, A.; Schmuki, P. Dye-sensitized anodic TiO₂ nanotubes. *Electrochem. Commun.* **2005**, *7*, 1133–1137. [[CrossRef](#)]
31. De Jong, H.; Van Pelt, A.; Arends, J. Contact Angle Measurements on Human Enamel—An in vitro Study of Influence of Pellicle and Storage Period. *J. Dent. Res.* **1982**, *61*, 11–13. [[CrossRef](#)] [[PubMed](#)]
32. Costanzo, P.; Giese, R.; Van Oss, C. Determination of the acid-base characteristics of clay mineral surfaces by contact angle measurements-implications for the adsorption of organic solutes from aqueous media. *J. Adhes. Sci. Technol.* **1990**, *4*, 267–275. [[CrossRef](#)]
33. Busscher, H.J. Wettability of Surfaces in the Oral Cavity. *Mod. Approaches Wettability* **1992**, *1992*, 249–261. [[CrossRef](#)]
34. Olsson, J.; Carlen, A.; Holmberg, K. Inhibition of *Streptococcus mutans* Adherence to Hydroxyapatite with Combinations of Alkyl Phosphates and Nonionic Surfactants. *Caries Res.* **1991**, *25*, 51–57. [[CrossRef](#)] [[PubMed](#)]
35. Tanner, J.; Robinson, C.; Söderling, E.; Vallittu, P. Early plaque formation on fibre-reinforced composites in vivo. *Clin. Oral Investig.* **2005**, *9*, 154–160. [[CrossRef](#)] [[PubMed](#)]
36. Ebi, N.; Imazato, S.; Noiri, Y.; Ebisu, S. Inhibitory effects of resin composite containing bactericide-immobilized filler on plaque accumulation. *Dent. Mater.* **2001**, *17*, 485–491. [[CrossRef](#)]
37. Wang, C.; Wang, X.; Lu, R.; Gao, S.; Ling, Y.; Chen, S. Responses of human gingival fibroblasts to superhydrophilic hydrogenated titanium dioxide nanotubes. *Colloids Surf. B Biointerfaces* **2021**, *198*, 111489. [[CrossRef](#)] [[PubMed](#)]
38. Singhatanadgit, W.; Toso, M.; Pratheepsawangwong, B.; Pimpin, A.; Srituravanich, W. Titanium dioxide nanotubes of defined diameter enhance mesenchymal stem cell proliferation via JNK- and ERK-dependent up-regulation of fibroblast growth factor-2 by T lymphocytes. *J. Biomater. Appl.* **2018**, *33*, 997–1010. [[CrossRef](#)]
39. Tang, T.; Peng, Z.; Ni, J.; Zheng, K.; Shen, Y.; Wang, X.; He, G.; Jin, S. Dual effects and mechanism of TiO₂ nanotube arrays in reducing bacterial colonization and enhancing C3H10T1/2 cell adhesion. *Int. J. Nanomed.* **2013**, *8*, 3093–3105. [[CrossRef](#)]
40. Park, J.; Bauer, S.; Pittrof, A.; Killian, M.S.; Schmuki, P.; von der Mark, K. Synergistic Control of Mesenchymal Stem Cell Differentiation by Nanoscale Surface Geometry and Immobilized Growth Factors on TiO₂ Nanotubes. *Small* **2012**, *8*, 98–107. [[CrossRef](#)]
41. Park, J.; Bauer, S.; Schlegel, K.A.; Neukam, F.W.; von der Mark, K.; Schmuki, P. TiO₂ Nanotube Surfaces: 15 nm-An Optimal Length Scale of Surface Topography for Cell Adhesion and Differentiation. *Small* **2009**, *5*, 666–671. [[CrossRef](#)]
42. Zwilling, V.; Aucouturier, M.; Darque-Ceretti, E. Anodic oxidation of titanium and TA6V alloy in chromic media. An electrochemical approach. *Electrochimica Acta* **1999**, *45*, 921–929. [[CrossRef](#)]
43. Anselme, K.; Davidson, P.; Popa, A.; Giazzone, M.; Liley, M.; Ploux, L. The interaction of cells and bacteria with surfaces structured at the nanometre scale. *Acta Biomater.* **2010**, *6*, 3824–3846. [[CrossRef](#)] [[PubMed](#)]
44. Lim, J.Y.; Donahue, H.J. Cell Sensing and Response to Micro- and Nanostructured Surfaces Produced by Chemical and Topographic Patterning. *Tissue Eng.* **2007**, *13*, 1879–1891. [[CrossRef](#)]
45. Minagar, S.; Wang, J.; Berndt, C.; Ivanova, E.; Wen, C. Cell response of anodized nanotubes on titanium and titanium alloys. *J. Biomed. Mater. Res. Part A* **2013**, *101*, 2726–2739. [[CrossRef](#)] [[PubMed](#)]
46. Wang, R.; Hashimoto, K.; Fujishima, A.; Chikuni, M.; Kojima, E.; Kitamura, A.; Shimohigoshi, M.; Watanabe, T. Light-induced amphiphilic surfaces. *Nature* **1997**, *388*, 431–432. [[CrossRef](#)]
47. Hori, N.; Ueno, T.; Suzuki, T.; Yamada, M.; Att, W.; Okada, S.; Ohno, A.; Aita, H.; Kimoto, K.; Ogawa, T. Ultraviolet light treatment for the restoration of age-related degradation of titanium bioactivity. *Int. J. Oral Maxillofac. Implants* **2010**, *25*, 49–62.
48. Dos Santos, E.A.; Farina, M.; Soares, G.A.; Anselme, K. Surface energy of hydroxyapatite and β -tricalcium phosphate ceramics driving serum protein adsorption and osteoblast adhesion. *J. Mater. Sci. Mater. Med.* **2008**, *19*, 2307–2316. [[CrossRef](#)]
49. Clark, A.J.; Kotlicki, A.; Haynes, C.A.; Whitehead, L.A. A New Model of Protein Adsorption Kinetics Derived from Simultaneous Measurement of Mass Loading and Changes in Surface Energy. *Langmuir* **2007**, *23*, 5591–5600. [[CrossRef](#)]
50. Noh, H.; Vogler, E.A. Volumetric interpretation of protein adsorption: Mass and energy balance for albumin adsorption to particulate adsorbents with incrementally increasing hydrophilicity. *Biomaterials* **2006**, *27*, 5801–5812. [[CrossRef](#)]
51. Ueno, T.; Yamada, M.; Suzuki, T.; Minamikawa, H.; Sato, N.; Hori, N.; Takeuchi, K.; Hattori, M.; Ogawa, T. Enhancement of bone–titanium integration profile with UV-photofunctionalized titanium in a gap healing model. *Biomaterials* **2010**, *31*, 1546–1557. [[CrossRef](#)]
52. Aita, H.; Att, W.; Ueno, T.; Yamada, M.; Hori, N.; Iwasa, F.; Tsukimura, N.; Ogawa, T. Ultraviolet light-mediated photofunctionalization of titanium to promote human mesenchymal stem cell migration, attachment, proliferation and differentiation. *Acta Biomater.* **2009**, *5*, 3247–3257. [[CrossRef](#)] [[PubMed](#)]

53. Att, W.; Hori, N.; Iwasa, F.; Yamada, M.; Ueno, T.; Ogawa, T. The effect of UV-photofunctionalization on the time-related bioactivity of titanium and chromium–cobalt alloys. *Biomaterials* **2009**, *30*, 4268–4276. [[CrossRef](#)]
54. Bollen, C.M.L.; Papaioanno, W.; Van Eldere, J.; Schepers, E.; Quirynen, M.; Van Steenberghe, D. The influence of abutment surface roughness on plaque accumulation and peri-implant mucositis. *Clin. Oral Implants Res.* **1996**, *7*, 201–211. [[CrossRef](#)]
55. Patel, S.B.; Baker, N.; Marques, I.; Hamlekhan, A.; Mathew, M.T.; Takoudis, C.; Friedrich, C.; Sukotjo, C.; Shokuhfar, T. Transparent TiO₂ nanotubes on zirconia for biomedical applications. *RSC Adv.* **2017**, *7*, 30397–30410. [[CrossRef](#)]
56. Rosqvist, E.; Niemelä, E.; Venu, A.P.; Kummala, R.; Ihalainen, P.; Toivakka, M.; Eriksson, J.E.; Peltonen, J. Human dermal fibroblast proliferation controlled by surface roughness of two-component nanostructured latex polymer coatings. *Colloids Surf. B Biointerfaces* **2019**, *174*, 136–144. [[CrossRef](#)] [[PubMed](#)]
57. Lassila, L.V.; Garoushi, S.; Tanner, J.; Vallittu, P.K.; Söderling, E. Adherence of Streptococcus mutans to Fiber-Reinforced Filling Composite and Conventional Restorative Materials. *Open Dent. J.* **2009**, *3*, 227–232. [[CrossRef](#)] [[PubMed](#)]
58. Suzuki, T.; Hori, N.; Att, W.; Kubo, K.; Iwasa, F.; Ueno, T.; Maeda, H.; Ogawa, T. Ultraviolet Treatment Overcomes Time-Related Degradation Bioactivity of Titanium. *Tissue Eng. Part A* **2009**, *15*, 3679–3688. [[CrossRef](#)]